NANO LETTERS

Letter

pubs.acs.org/NanoLett

# All-Optical Logic Gates Based on Nanoscale Plasmonic Slot Waveguides

Yulan Fu, Xiaoyong Hu,* Cuicui Lu, Song Yue, Hong Yang, and Qihuang Gong*

State Key Laboratory for Mesoscopic Physics & Department of Physics, Peking University, Beijing 100871, People's Republic of China

**ABSTRACT:** We report realizations of nanoscale integrated all-optical XNOR, XOR, NOT, and OR logic gates using plasmonic slot waveguides based on linear interference between surface plasmon polariton modes. The miniature device size with lateral dimensions smaller than 5 $\mu$m, precisely controlled optical phase difference, and quasi-monochromatic surface plasmon polariton modes excited by a continuous wave 830 nm laser beam ensure a high intensity contrast ratio of 24 dB between the output logic states "1" and "0". Compared with previous reported results, the intensity contrast ratio is enhanced 4-fold, whereas the lateral dimension is reduced 4-fold. These compact logic devices are stable, robust, free from environmental impact, and much suitable for practical on-chip applications. These also provide a means to construct all-optical logic devices and nanophotonic processors.

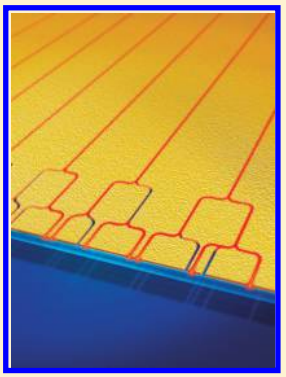

**KEYWORDS:** *Surface plasmon polaritons, all-optical logic gates, plasmonic slot waveguide, linear interference effect*

Recently, nanoscale all-optical logic gate devices have attracted enormous attention because of their important applications in fields of optical computing and ultrahigh speed information processing. The basic idea is to form constructive/destructive interference between two light signals in a photonic crystal, a photonic microstructure having photonic bandgap, to obtain output logic states "1" and "0", where the phase difference is introduced through third-order optical nonlinearity.[1−3] However, to date, few experimental results of nanoscale integrated all-optical logic gate devices have been reported because of small third-order nonlinear susceptibility of conventional materials.[4] Linear interference can also be used to realize such logic gate devices, where the logic operation depends on the relative optical phase difference of two input signals.[5] Owing to the difficulty in precisely controlling the optical phase difference, this method suffers from an inherent instability and low intensity contrast ratio between output logic states "1" and "0".[6] Until now, only a few experimental results have been reported.[6] It is possible to reduce the inherent instability by device miniaturization and monolithic integration.[7] Plasmonic microstructures can confine light into subwavelength-scale regions and exhibit strong plasmonic enhancement, which provides an approach to scale down photonic devices further and to realize direct integration with solid-state chips.[8,9] Recently, Wei et al. have reported several all-optical logic gates based on linear interference between surface plasmon polariton (SPP) modes in a silver nanowire network.[10,11] The length of silver nanowires was about 20 $\mu$m, and the achieved intensity contrast ratio of output logic states "1" and "0" was only 6 dB.[10,11]

Here, we propose and realize nanoscale integrated all-optical XNOR, XOR, NOT, and OR logic gates based on the linear interference of SPP modes in plasmonic slot waveguides, consisting of air slots etched in a thin gold film. These structures can provide transverse-magnetic (TM)-like SPP modes, also called quasi-TEM SPP modes, strongly confined at the interface of dielectric waveguide and metal films.[12] The plasmonic slot waveguide exhibits both ultralong range propagation of over several tens of micrometers and strong spatial confinement of light into a subwavelength scale region.[13] SPP modes propagate in the direction parallel to gold film, which is suitable for on-chip integration applications. The miniature device featuring lateral dimensions of less than 5 $\mu$m, precisely controlled optical phase differences obtained through exact patterning of logic gates using focused ion-beam (FIB) etching technology, and quasi-monochromatic SPP modes excited by an 830 nm continuous-wave (CW) laser beam ensure a high intensity contrast ratio of 24 dB between output logic states "1" and "0". These compact logic devices are stable, robust, and free from environmental impact, meeting the requirements of practical on-chip integration applications.

The schematic structure of the plasmonic slot waveguide is shown in Figure 1a. It consists of an air slot with width $w$ of 100 nm etched in a gold film with thickness $h$ of 100 nm on a silicon dioxide substrate. The dispersion relation of the plasmonic slot waveguide was calculated by the finite element method (using a commercial software package Comsol Multiphysics),[14] and the calculated results are depicted in Figure 1b. The refractive index of air and silicon dioxide was set at 1 and 1.5, respectively. The wavelength-dependent complex

**Received:** August 20, 2012
**Revised:** October 15, 2012





dx.doi.org/10.1021/nl303095s | *Nano Lett.* XXXX, XXX, XXX−XXX

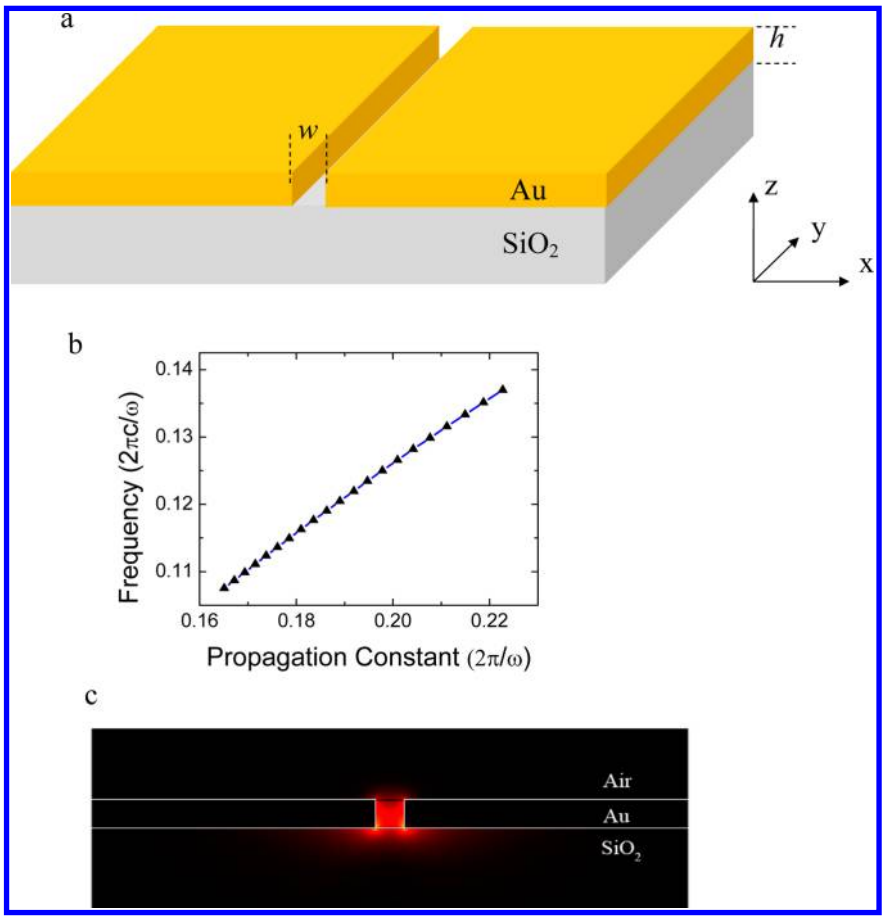


**Figure 1.** Characteristics of the plasmonic slot waveguide. (a) Schematic structure. (b) Dispersion relation. (c) Power density profile of a 530 nm SPP mode.

refractive index of gold was obtained from ref 15. The plasmonic slot waveguide can provide wideband guided SPP modes, which has been confirmed by Dionne's calculations.[13] To further confirm the guided SPP modes, we also calculated the power density profile of a 530 nm guided mode by the finite element method, and the calculated results are shown in Figure 1c. The guided mode is confined mostly in the slot region and extends slightly into the adjacent silicon dioxide and air regions. The maximum intensity is at the gold−air interface in the slot, which is in agreement with Dionne's calculations.[13] The effective refractive index of the plasmonic slot waveguide for a 530 nm SPP mode was calculated to be 1.57 + 0.0106*i*, which indicates that the effective propagating length of this SPP mode is 11 $\mu$m.

Gold films with a thickness of 100 nm were prepared using a laser molecular beam epitaxy (LMBE) growth system (model LMBE 450, SKY Company, China). As the excitation light source, we used the beam (with a wavelength of 248 nm, a pulse width of 25 ns, and a pulse repetition rate of 5 Hz) output from an excimer laser system (model ComPexPro 205, Coherent Company, USA). A FIB etching system (model DB235, FEI Company, USA) was employed to prepare the logic gate patterns. All widths of the plasmonic slot waveguides were 100 nm. To excite and collect the needed SPP mode, we also etched a coupling grating connected with an air groove with a triangular configuration at the input port of each plasmonic slot waveguide. We also etched a grating in the output port to help couple the SPP mode to free space for the purpose of measurement. The scanning electron microscopy (SEM) images of the fabricated logic gate samples are shown in Figure 2. The lateral dimension of the logic gate devices was less than 5 $\mu$m, reduced 4-fold compared with those used in previous reports.[10,11] The all-optical logic functions were measured using a scanning near-field optical microscopy

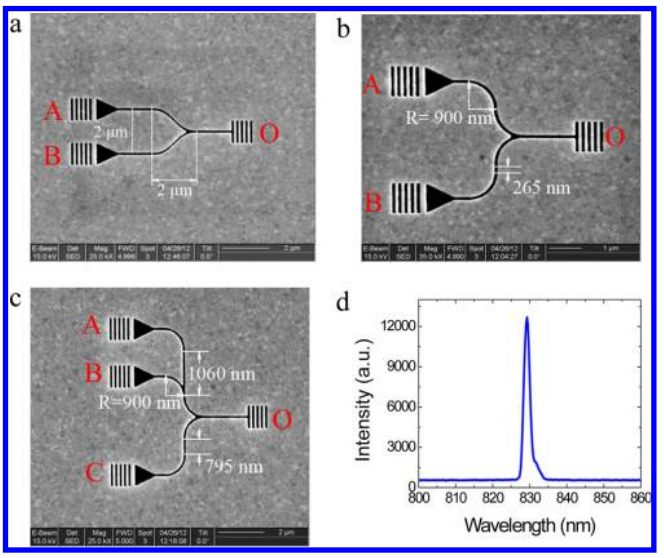


**Figure 2.** SEM images of all-optical logic gate samples. (a) For the OR gate. (b) For the NOT gate. (c) For the XNOR gate. (d) Laser spectrum.


dx.doi.org/10.1021/nl303095s | *Nano Lett.* XXXX, XXX, XXX−XXX

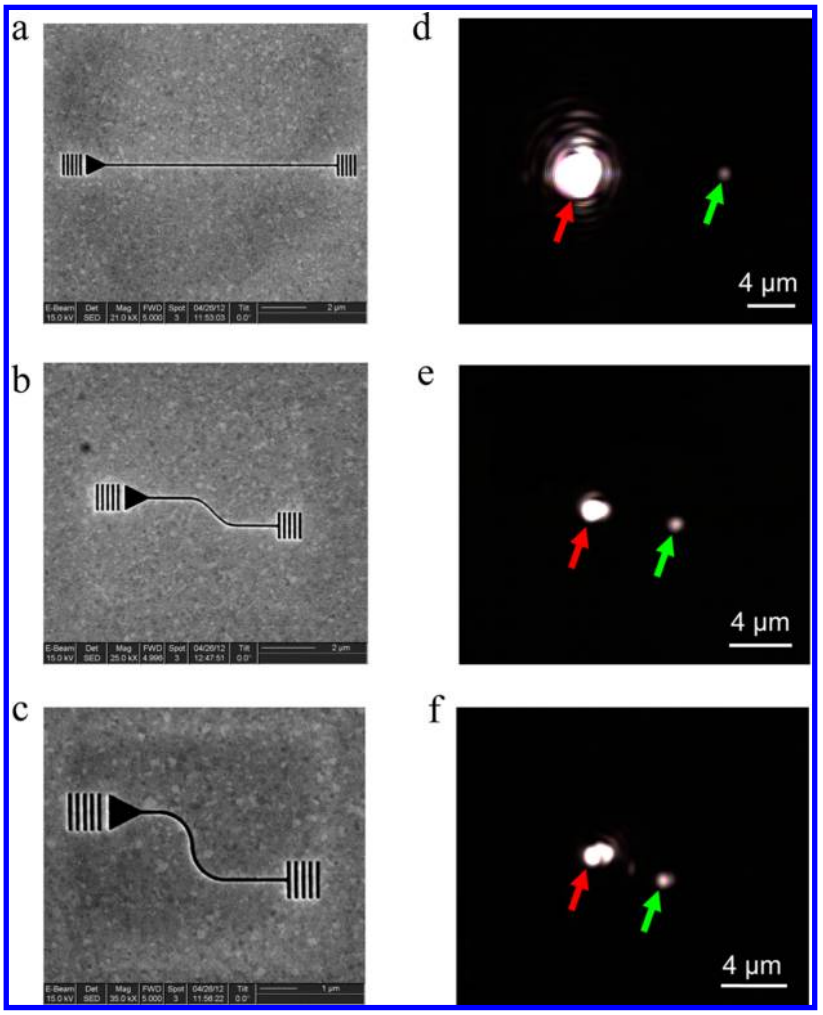


**Figure 3.** SEM images of plasmonic slot waveguides with a width of 100 nm and a length of 11 $\mu$m for a straight waveguide (a), a 90° circle arc waveguide with a radius of 900 nm (b), and a cosine arc-shaped waveguide (c). CCD images of plasmonic slot waveguide under excitation of an 830 nm CW laser for the straight waveguide (d), the 90° circle arc waveguide with a radius of 900 nm (e), and the cosine arc shape waveguide (f). The red arrow indicates the position of the coupling grating in the input port of the plasmonic slot waveguide. The green arrow indicates the position of the decoupling grating in the output port of the plasmonic slot waveguide.

system. The input coupling grating was normally illuminated from the back side using a p-polarized CW Ti:sapphire laser beam with a wavelength of 830 nm. The incident laser beam was focused into a spot with a radius of about 2.5 $\mu$m, ensuring that the laser beam covers all input gratings. The spot center was set at the perpendicular bisector line of the connection line between two input coupling gratings. The patterned area of each input coupling grating was about 1 $\mu$m × 1 $\mu$m. This ensures a nearly equal average excitation intensity for all of the input coupling gratings. The spectrum of the 830 nm laser beam is shown in Figure 2d. The line width of the laser spectrum curve was only 1.9 nm, which ensured that only the needed quasi-monochromatic 530 nm SPP mode can be excited in the plasmonic slot waveguide. The optical-thick gold film can prevent the direct transmission of the laser beam. The incident laser was coupled into a 530 nm SPP mode through the input grating. The SPP mode propagating through the plasmonic slot waveguide was scattered by the decoupling grating in the output port. The scattered light was collected by a long working distance objective (Mitutoyo 20, NA = 0.58) and then imaged onto a charge coupled device (CCD). To confirm the propagation properties of the SPP mode in the plasmonic slot waveguide, we also etched a straight waveguide, a 90° circular arc waveguide with a radius of 900 nm, and a cosine arc-shaped waveguide, as shown in Figure 3a–c. The width and length of each of the three kinds of plasmonic slot waveguides were 100 nm and 11 $\mu$m, respectively. It is very clear that, under excitation of an 830 nm CW laser, there is a distinctive signal output from the decoupling grating for each kind of waveguide, as shown in Figure 3d–f. This confirms the excellent propagation properties of the 530 nm SPP mode. The different sizes of laser spot in Figure 3d–f are related to the different excitation intensity.

The XNOR gate has three input waveguides, as shown in Figure 2c, the bending regions of which having a circular arc shape with a radius of 900 nm to reduce propagation losses.[16] There is an optical path difference of 795 nm between waveguides B and C, and 265 nm between waveguides A and C. Therefore, a destructive interference can be reached in the output waveguide for the 530 nm SPP modes propagating through waveguides A and C, or waveguides B and C, while a constructive interference can be reached for the 530 nm SPP modes propagating through waveguides A and B. Waveguide C was used as the reference waveguide. To perform the logic operation of "0 XNOR 0=1", we etched a coupling grating connected with a triangular air groove in the input port of


dx.doi.org/10.1021/nl303095s | *Nano Lett.* XXXX, XXX, XXX–XXX

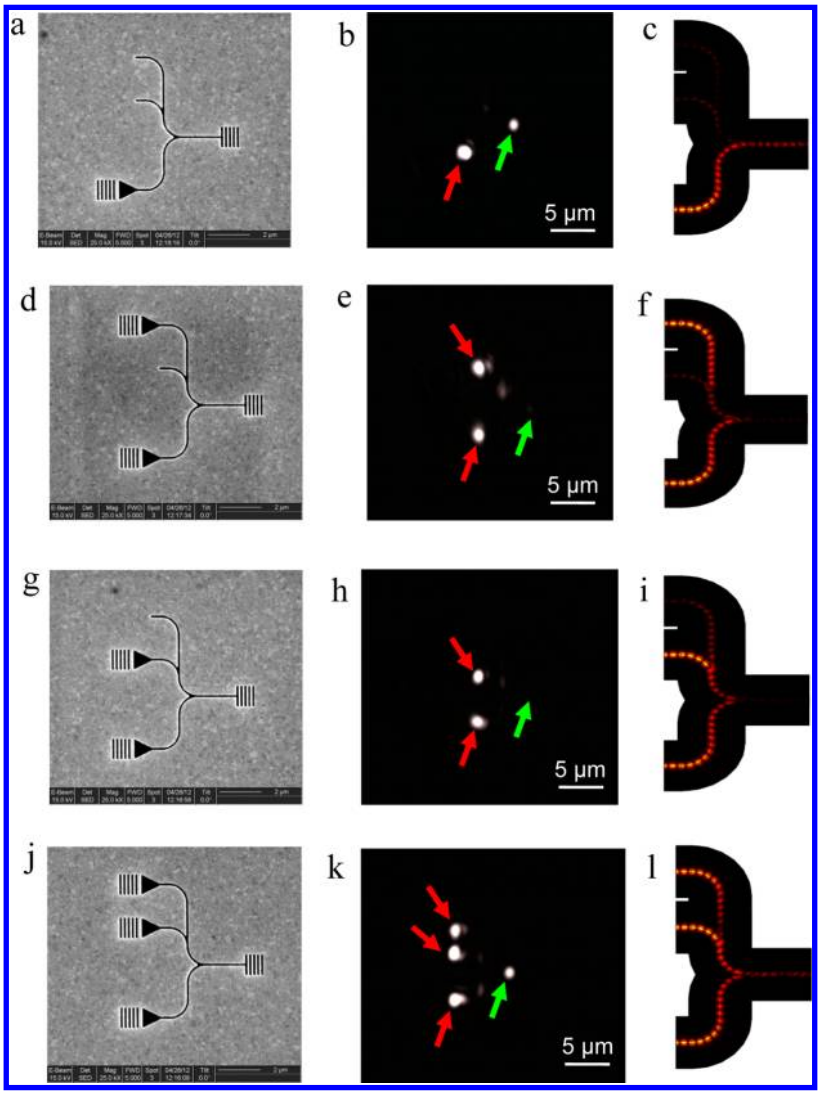


**Figure 4.** Logic operation of XNOR gate. The SEM image of sample (a), measured CCD image under excitation of an 830 nm CW laser (b), and simulated results (c) for the logic operation of "0 XNOR 0=1". The SEM image of sample (d), measured CCD image under excitation of an 830 nm CW laser (e), and simulated results (f) for the logic operation of "1 XNOR 0=0". The SEM image of sample (g), measured CCD image under excitation of an 830 nm CW laser (h), and simulated results (i) for the logic operation of "0 XNOR 1=0". The SEM image of sample (j), measured CCD image under excitation of an 830 nm CW laser (k), and simulated results (l) for the logic operation of "1 XNOR 1=1". The red arrow indicates the position of the coupling grating in the input port of the plasmonic slot waveguide. The green arrow indicates the position of the decoupling grating in the output port of the plasmonic slot waveguide.

waveguide C, as shown in Figure 4a. The 530 nm SPP mode can only be excited in waveguide C. No SPP mode can be excited in waveguides A and B. The measured CCD image obtained under excitation of an 830 nm CW laser is shown in Figure 4b. There is strong signal with an intensity of 2.09 au output from the decoupling grating. This corresponds to output logic "1". The simulated $H_z$ field distribution when the SPP mode is incident in waveguide C is shown in Figure 4c. A strong signal output can be obtained in the output port, thus confirming the measured results. To perform the logic operation of "1 XNOR 0=0", we etched a coupling grating connected with a triangular air groove in the input port of both waveguides A and C, as shown in Figure 4d. The 530 nm SPP mode can be excited in waveguides A and C simultaneously. The measured CCD image obtained under excitation of an 830 nm CW laser is shown in Figure 4e. There is a very weak signal with an intensity of 0.00725 au output from the decoupling grating. This corresponds to output logic "0". The reason is that a destructive interference is reached in the output waveguide for SPP modes propagating through waveguides A and C because the optical path difference is a half of the wavelength of the SPP mode. The simulated $H_z$ field distribution when SPP mode is incident in waveguides A and C is shown in Figure 4f. No signal can be obtained from the output waveguide. This confirms the logic operation of "1 XNOR 0=0". To perform the logic operation of "0 XNOR 1=0", we etched a coupling grating connected with a triangular air groove in the input port of both waveguides B and C, as shown in Figure 4g. Thus, the 530 nm SPP mode can be excited in both these waveguides simultaneously. The measured CCD image obtained under excitation of an 830 nm CW laser is shown in Figure 4h. There is a very weak signal output from the decoupling grating with an intensity of 0.00916 au. This corresponds to the output logic "0". The reason is that a destructive interference is reached at the output waveguide for SPP modes propagating through waveguides B and C because the optical path difference is one


dx.doi.org/10.1021/nl303095s | *Nano Lett.* XXXX, XXX, XXX–XXX

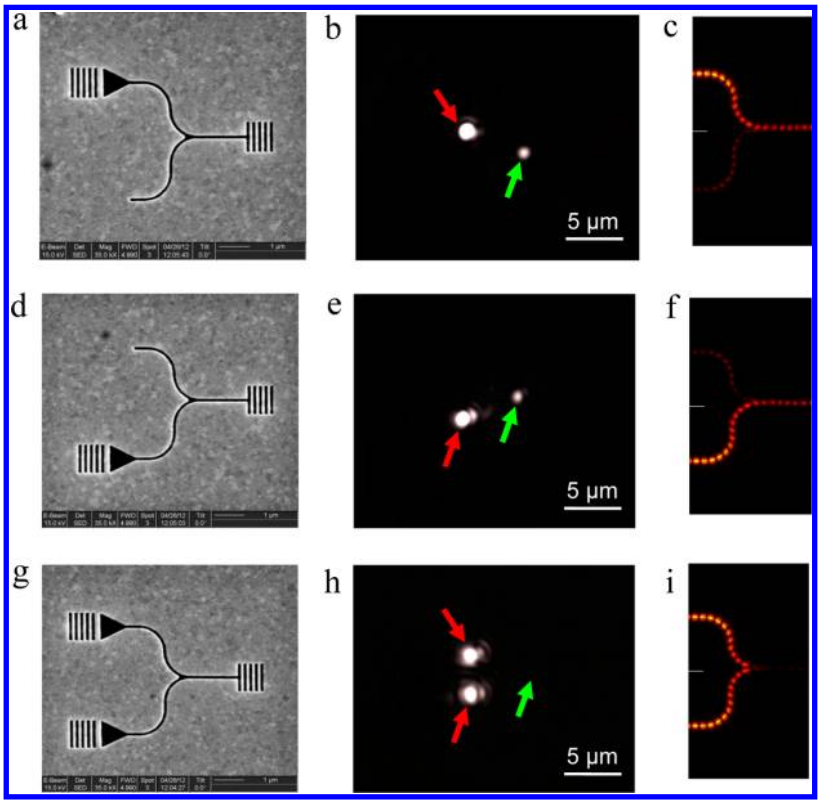


**Figure 5.** Logic operation of XOR gate. The SEM image of sample (a), measured CCD image under excitation of an 830 nm CW laser (b), and simulated results (c) for the logic operation of "1 XOR 0=1". The SEM image of sample (d), measured CCD image under excitation of an 830 nm CW laser (e), and simulated results (f) for the logic operation of "0 XOR 1=1". The SEM image of sample (g), measured CCD image under excitation of an 830 nm CW laser (h), and simulated results (i) for the logic operation of "1 XOR 1=0". The red arrow indicates the position of the coupling grating in the input port of the plasmonic slot waveguide. The green arrow indicates the position of the decoupling grating in the output port of the plasmonic slot waveguide.

and a half of the SPP wavelength. The simulated $H_z$ field distribution when the SPP mode is incident in waveguides B and C is shown in Figure 4i. No signal can be obtained from the output waveguide. This confirms the logic operation of "0 XNOR 1=0". To perform the logic operation of "1 XNOR 1=1", we etched a coupling grating connected with a triangular air groove in the input ports of all waveguides A, B, and C, as shown in Figure 4j. The SPP mode can be excited in all three waveguides simultaneously. The measured CCD image obtained under excitation of an 830 nm CW laser is shown in Figure 4k. There is a strong signal output from the decoupling grating with an intensity of 2.193 au. This corresponds to the output logic "1". Here, the total intensity of SPP mode propagating through waveguides A and B is double that in waveguide C. Although a part of the SPP energy in the output waveguide is reduced through destructive interference, the remainder can still be obtained from the output waveguide. The simulated $H_z$ field distribution when SPP modes are incident in waveguides A, B, and C simultaneously is shown in Figure 4l. A strong signal can be obtained from the output waveguide. This confirms the logic operation of "1 XNOR 1=1". The intensity contrast ratio between the output logic "1" and "0" can be calculated from $10\cdot\log(P_1/P_0)$, where $P_1$ and $P_0$ are the signal intensities of logic "1" and "0", respectively.[4,5] The intensity contrast ratio between output logic "1" and "0" was measured to be 24.8 dB, which is enhanced by 4-fold compared with previously experimental reports.[10,11] When the guided SPP mode propagates in the direction of *Y*-axis, as shown in Figure 1a, the guided SPP mode can be described in the form of[17]

$$\vec{H}(\vec{r}, t) = \vec{H_0}(x, y)e^{i(\beta y-\omega t)} \quad (1)$$

where $\beta$ is the propagation constant and $\omega$ the circular frequency of the guided SPP mode. Therefore, the $H_z$ field distribution of the guided SPP mode takes on a standing-wave-like pattern (Figure 4c, f, i, and l) due to the modulation action of the term $e^{i(\beta y-\omega t)}$.[18]

The XOR gate has an asymmetric Y-shape configuration, as shown in Figure 2b, the bending region of which has a circular arc shape with a radius of 900 nm to reduce propagation losses.[16] There is an optical path difference of 265 nm between waveguides A and B, which indicates that a destructive interference can be reached in the output waveguide for 530 nm SPP modes propagating through waveguides A and B. When a signal light was input in one of the input waveguides, a strong signal was obtained in the output port. Therefore, the logic operations of "1 XOR 0=1" (Figure 5a,b) and "0 XOR 1=1" (Figure 5d,e) were realized. There is a strong signal with an intensity of 5.043 au output from the decoupling grating, which corresponds to output logic "1". When signal light was input in waveguides A and B simultaneously, no signal was obtained in the output port because a destructive interference was reached in the output waveguide. Therefore, the logic operation of "1 XOR 1=0" (Figure 5g,h) was realized. There is a very weak signal output from the decoupling grating with an intensity of 0.0342 au, which corresponds to output logic "0". The measured intensity contrast ratio reached 21.7 dB. The


dx.doi.org/10.1021/nl303095s | *Nano Lett.* XXXX, XXX, XXX–XXX

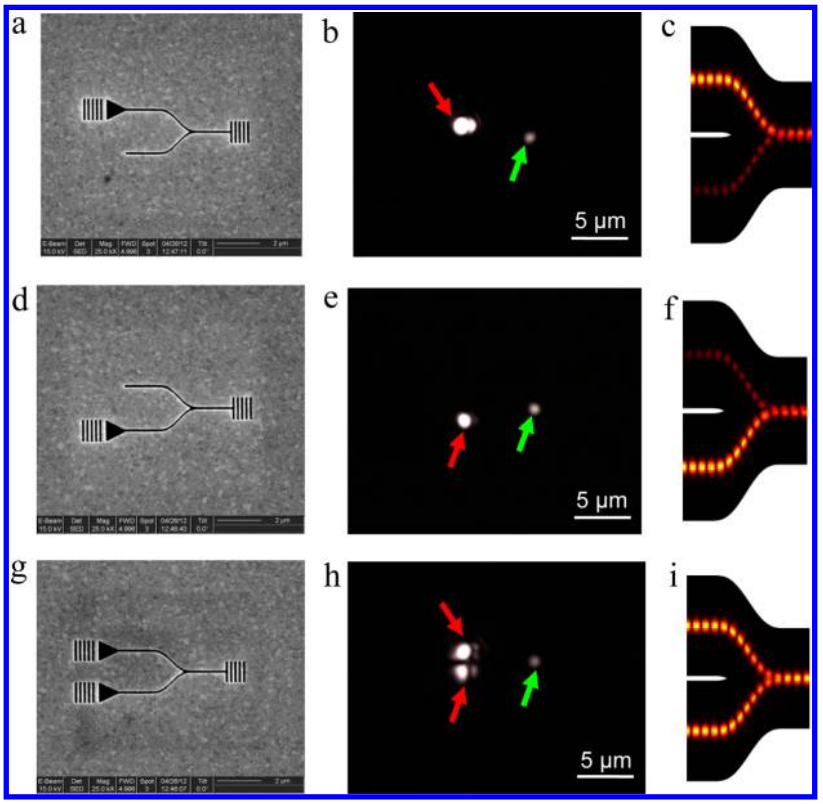


**Figure 6.** Logic operation of OR gate. The SEM image of sample (a), measured CCD image under excitation of an 830 nm CW laser (b), and simulated results (c) for the logic operation of "1 OR 0=1". The SEM image of sample (d), measured CCD image under excitation of an 830 nm CW laser (e), and simulated results (f) for the logic operation of "0 OR 1=1". The SEM image of sample (g), measured CCD image under excitation of an 830 nm CW laser (h), and simulated results (i) for the logic operation of "1 OR 1=1". The red arrow indicates the position of the coupling grating in the input port of the plasmonic slot waveguide. The green arrow indicates the position of the decoupling grating in the output port of the plasmonic slot waveguide.

measured logic performances are in agreement with the calculated ones, as shown in Figure 5c, f, and i. If we set waveguide B as a reference waveguide, a NOT gate can be realized very easily by using the same configuration of the XOR gate. For example, the sample shown in Figure 5d can be used to fulfill logic operation "NOT 0=1" (Figure 5e,f). The sample shown in Figure 5g can be used to fulfill logic operation "NOT 1=0" (Figure 5h,i).

The OR gate has a symmetric Y-shape configuration, as shown in Figure 2a, the bending regions of which having a cosine-arc shape so as to ensure small propagation losses.[16] The distance between waveguides A and B was 2 $\mu$m. The length of the bended waveguide was also 2 $\mu$m. The distance from the input port of either waveguide to the interaction point has exactly the same value, which will ensure constructive interference in the output waveguide. When a signal light was input in one of the waveguides, a strong signal was obtained in the output port. Therefore, the logic operations of "1 OR 0=1" (Figure 6a,b) and "0 OR 1=1" (Figure 6d,e) were realized. When a signal light was input in waveguides A and B simultaneously, a strong signal was obtained in the output port because a constructive interference was reached in the output waveguide. Therefore, the logic operation of "1 OR 1=1" (Figure 6g,h) was realized. The measured logic performances are in agreement with those calculated ones shown in Figure 6c, f, and i.

One shortcoming of plasmonic slot waveguides, that is, that their performances will be influenced if dust or small nanoparticles fall into the air slots, can be overcome by filling the air slots with dielectric material.[18] According to our calculation, no cross-talk occurs when the distance between two plasmonic slot waveguides is larger than 200 nm. This has been confirmed by Gramotnev's measured results.[19] Various integrated photonic devices have been demonstrated based on plasmonic slot waveguides, such as plasmonic splitters,[20] modulators,[21] and directional couplers.[17] Therefore, plasmonic slot waveguide is very promising for the future dense on-chip integration applications.

In conclusion, four nanoscale integrated all-optical logic gates have been demonstrated XNOR, XOR, NOT, and OR functions, based on the linear interference effect of SPP modes. The intensity contrast ratio between the output logic "1" and "0" reached as high as 24 dB, and the lateral dimension was reduced to less than 5 $\mu$m. This may offer a simple and effective approach for the realization of nanoscale integrated SPP all-optical logic devices suitable for on-chip applications.

## AUTHOR INFORMATION

### Corresponding Author

*E-mail: xiaoyonghu@pku.edu.cn (X. Hu); qhgong@pku.edu.cn (Q. Gong).

### Notes

The authors declare no competing financial interest.

## ACKNOWLEDGMENTS

This work was supported by the National Key Basic Research Program of China under grant 2013CB328704, the National

Natural Science Foundation of China under grants 61077027, 11134001, 11121091, and 90921008, and the program for New Century Excellent Talents in University.

## REFERENCES

(1) Mccutcheon, M. W.; Rieger, G. W.; Young, J. F.; Dalacu, D.; Poole, P. J.; Williams, R. L. All-optical conditional logic with a nonlinear photonic crystal nanocavity. *Appl. Phys. Lett.* **2009**, *95*, 221102.
(2) Zhu, Z. H.; Ye, W. M.; Ji, J. R.; Yuan, X. D.; Zen, C. High-contrast light-by-light switching and AND gate based on nonlinear photonic crystals. *Opt. Express* **2006**, *14*, 1783−1788.
(3) Liu, Q.; Ouyang, Z. B.; Wu, C. J.; Liu, C. P.; Wang, J. C. All-optical half adder based on cross structures in two-dimensional photonic crystals. *Opt. Express* **2008**, *16*, 18992−19000.
(4) Liu, Y.; Qin, F.; Meng, Z. M.; Zhou, F.; Mao, Q. H.; Li, Z. Y. All-optical logic gates based on two-dimensional low-refractive-index nonlinear photonic crystal slabs. *Opt. Express* **2011**, *19*, 1945−1953.
(5) Zhang, Y. L.; Zhang, Y.; Li, B. J. Optical switches and logic gates based on self-collimated beams in two-dimensional photonic crystals. *Opt. Express* **2007**, *15*, 9287−9292.
(6) Li, Z. J.; Chen, Z. W.; Li, B. J. Optical pulse controlled all-optical logic gates in SiGe/Si multimode interference. *Opt. Express* **2005**, *13*, 1033−1038.
(7) Caulfield, H. J.; Vikram, C. S.; Zavalin, A. Optical logic redux. *Optik* **2006**, *117*, 199−209.
(8) Barnes, W. L.; Dereux, A.; Ebbesen, T. W. Surface plasmon subwavelength optics. *Nature* **2003**, *424*, 824−830.
(9) Zhang, J. F.; Macdonald, K. F.; Zheludev, N. I. Controlling light-with-light without nonlinearity. *Light: Sci. Appl.* **2012**, *1*, e18.
(10) Wei, H.; Wang, Z. X.; Tian, X. R.; Kall, M.; Xu, H. X. Cascaded logic gates in nanophotonic plasmon networks. *Nat. Commun.* **2011**, *2*, 387.
(11) Wei, H.; Li, Z. P.; Tian, X. R.; Wang, Z. X.; Cong, F. Z.; Liu, N.; Zhang, S. P.; Nordlander, P.; Halas, J. N.; Xu, H. X. Quantum dot-based local field imaging reveals plasmon-based interferometric logic in silver nanowire networks. *Nano Lett.* **2011**, *11*, 471−475.
(12) Veronis, G.; Fan, S. H. Guided subwavelength plasmonic mode supported by a slot in a thin metal film. *Opt. Lett.* **2005**, *30*, 3359−3361.
(13) Dionne, J. A.; Sweatlock, L. A.; Atwater, H. A.; Polman, A. Plasmon slot waveguides: Towards chip-scale propagation with subwavelength-scale localization. *Phys. Rev. B* **2006**, *73*, 035407.
(14) Chen, J. J.; Li, Z.; Yue, S.; Gong, Q. H. Highly efficient all-optical control of surface-plasmon-polariton generation based on a compact asymmetric single slit. *Nano Lett.* **2011**, *11*, 2933−2937.
(15) Johnson, P. B.; Christy, R. W. Optical constants of the noble metals. *Phys. Rev. B* **1972**, *6*, 4370−4379.
(16) Volkov, V. S.; Bozhevolnyi, S. I.; Devaux, E.; Ebbesen, T. W. Compact gradual bends for channel plasmon polaritons. *Opt. Express* **2006**, *14*, 4494−4503.
(17) Salgueiro, J. R.; Kivshar, Y. S. Nonlinear plasmonic directional couplers. *Appl. Phys. Lett.* **2010**, *97*, 081106.
(18) Davoyan, A. R.; Shadrivov, I. V.; Zharov, A. A.; Gramotnev, D. K.; Kivshar, Y. S. Nonlinear nanofocusing in tapered plasmonic waveguide. *Phys. Rev. Lett.* **2010**, *105*, 116804.
(19) Gramotnev, D. K.; Nielsen, M. G.; Tan, S. J.; Kurth, M. L. Gap surface plasmon waveguides with enhanced integration and functionality. *Nano Lett.* **2012**, *12*, 359−363.
(20) Zhu, S. Y.; Lo, G. Q.; Kwong, D. L. Nanoplasmonic power splitters based on the horizontal nanoplasmonic slot waveguide. *Appl. Phys. Lett.* **2011**, *99*, 031112.
(21) Zhu, S. Y.; Lo, G. Q.; Kwong, D. L. Electro-absorption modulation in horizontal metal-insulator-silicon-insulator-metal nanoplasmonic slot waveguides. *Appl. Phys. Lett.* **2011**, *99*, 151114.